Available online at www.sciencedirect.com

jmr&t Journal of Materials Research and Technology

journal homepage: www.elsevier.com/locate/jmrt

Original Article

Development of a porous Ti–35Nb–5In alloy with low elastic modulus for biomedical implants

L. Romero-Resendiz [a,b,*], M.C. Rossi [b,c], C. Seguí-Esquembre [b], V. Amigó-Borrás [b]

[a] Facultad de Química, Departamento de Ingeniería Metalúrgica, Universidad Nacional Autónoma de México, Mexico City, 04510, Mexico

[b] Universitat Politècnica de València, Instituto de Tecnología de Materiales, Camino de Vera S/n, 46022 Valencia, Spain

[c] Department of Materials Engineering (DEMa), Universidade Federal de São Carlos (UFSCar), 13565-905, São Carlos - SP, Brazil

ARTICLE INFO

Article history:
Received 19 September 2022
Received in revised form
23 November 2022
Accepted 3 December 2022
Available online 7 December 2022

Keywords:
Ti alloy
Mechanical properties
Ion release
Corrosion
Microstructure

ABSTRACT

A new porous Ti–35Nb–5In alloy was designed to join the advantages of low elastic modulus and non-toxicity, which are critical factors for biomedical implants. The Ti–35Nb–5In alloy was produced by powder metallurgy, and its feasibility as implant material was evaluated through mechanical properties, ion release, and electrochemical assessments. The microstructure of the Ti–35Nb–5In alloy consisted of acicular α-phase and fine α''-phase within a micrometric β-phase matrix. A low elastic modulus of 63 GPa, as well as hardness and flexural strengths higher than the reported for the human bone, ensured the mechanical adequacy of the alloy. The Ti, Nb, and In releases were below toxic levels for the human body. The electrochemical performance showed the formation of a surface passive layer formation that encouraged a low corrosion rate. The corrosion performance was mainly influenced by chemical heterogeneities (preferred dissolution of Nb segregates) and porosity. Based on the above, the porous Ti–35Nb–5In alloy was demonstrated as a promising candidate for biomedical implant applications.

1. Introduction

Biocompatible and mechanically efficient materials for biomedical implants constitute an immediate challenge to attend around the world. A fast-increasing demand for biomedical implants is continuously expected [1–3]. The β-Ti alloys are recognized as the most promising materials for biomedical implants due to their low elastic modulus and good biocompatibility resulting from the use of non-toxic alloying β-stabilizers [4]. The low elastic modulus, as near as possible to the one of the human bone, is a key factor in

* Corresponding author. Facultad de Química, Departamento de Ingeniería Metalúrgica, Universidad Nacional Autónoma de México, Mexico City, 04510, Mexico
E-mail address: liliana.rom7@comunidad.unam.mx (L. Romero-Resendiz).

https://doi.org/10.1016/j.jmrt.2022.12.011

decreasing the mechanical mismatch between the implant and bone [5]. The low mechanical mismatch avoids disuse osteoporosis and stress shielding to the bone, increasing the success rate of the implant [6,7].

Besides β microstructures, porosity in Ti alloys also encourages low elastic modulus and promotes the fixation and osseointegration of the organic tissue with the metallic implant [8,9]. However, high porosity can decrease the corrosion resistance of Ti alloys [10]. Thus, a processing technique that allows good porosity control is required. Powder metallurgy and additive manufacturing are widely used techniques to produce alloys with functional porosity that improve the success rate of biomaterials [11–13]. However, the former one may be more advantageous in terms of feedstock cost and lower surface roughness [14,15]. Furthermore, the conventional press and sintering (P&S) technique is the most cost-competitive of the powder metallurgy methods [16].

Seeking biocompatibility and low elastic modulus materials, several porous β-Ti or near-β-Ti alloys have been reported. Examples of the above are Ti-Nb [17,18], Ti-Sn [19], Ti-Nb-Sn [20–22], Ti-In Ref. [23], Ti-Mo [24,25], Ti-Nb-Zr [26], Ti-Nb-Ta-Zr [27], Ti-Nb-Zr-Sn [28], and Ti–Mo–Zr [25]. From the abovementioned reports, the lowest elastic modulus belongs to the porous Ti–Nb-X systems with Nb content from 16 to 35 wt%, i.e., Ti–35Nb–2Ta–3Zr (3.1–3.9 GPa) [27], Ti–24Nb–4Zr–8Sn (0.9–1.3 GPa) [28], Ti–35Nb and Ti–16Nb (15–97 GPa) [17,18] and Ti–34Nb–6Sn, Ti–35Nb–2Sn, and Ti–16Nb–2Sn (14–78 GPa) [20–22]. It is noteworthy that Nb encourages low elastic moduli in Ti-alloys. Besides, Nb coatings have been reported as biocompatible and bioinert in materials for metallic implants [29]. However, high ionic Nb concentrations can harm human health [30]. The ion Nb release from Ti-alloys with 34 wt% Nb is within safe levels for the human body [20].

From the above, Nb is a promising alloying element to be combined with the non-toxicity, free-allergy, and good electrochemical performance of In [31,32]. Porous Ti–In alloys with In contents from 2.5 to 10 wt% have reported ion release levels below toxic concentrations as well as adequate mechanical properties for resisting permanent deformation without risky opposition to teeth [23]. Furthermore, it has been reported that In additions encourage low elastic modulus due to lattice expansion and weakening of chemical bonds [33]. As expected, yield strength might also decrease with the In additions [33]. Thus, small In additions that encourage low elastic modulus, stable β phase, and adequate yield strength should be selected.

Despite the advantages of Nb and In as alloying elements for Ti biomedical alloys, there is scarce information on porous Ti–Nb–In alloys. From the literature, cast (dense) Ti–40Nb–4In showed high biocompatibility, minor metal ion release, non-negative effect on corrosion stability, and spontaneous passive oxide layer formation [34,35]. The Ti–Nb–In alloy may be further improved by decreasing the elastic modulus expected in dense alloys. Despite the elastic modulus of the Ti–Nb–In system has not been reported yet, it is expected that powder metallurgy-processed Ti alloys have a remarkable decrement compared to their dense counterparts. An example of the above is the Ti–15Mo alloy with elastic modulus from 5 to 50 GPa [36] in the porous conditions and 78 GPa in the dense annealed condition [37]. Thus, studying porous Ti–Nb–In alloys might provide a new biocompatible route for implant efficiency by lower elastic modulus and enhanced osseointegration compared to the dense alloy.

The objective of this work is to design and produce a new porous Ti–Nb–In alloy that improves the reported dense Ti–40Nb–4In alloy through a low elastic modulus and suitable mechanical behavior for medical implants. To combine the abovementioned properties and maintain the non-toxicity, a porous Ti–35Nb–5In alloy was produced by powder metallurgy. Mechanical, electrochemical, and ion release evaluation were performed to determine the feasibility of the new alloy for orthopedic and dental implants. Comparisons with other β-Ti from the literature are included to remark on the advantages of the new porous Ti–35Nb–5In alloy. The development of this new porous alloy may mark a tendency to explore different non-toxic, biocompatible, and mechanically feasible alloy systems for biomedical purposes.

2. Experimental procedure

2.1. Elaboration of the alloy

Elemental powders of Ti, Nb, and In were purchased from Atlantic Equipment Engineers and Alpha Aesar and weighed according to the stoichiometric composition of the Ti–35Nb–5In (wt.%) alloy. As explained in the introduction, the Nb and In contents were selected to encourage low elastic modulus and metallic ion release within safe ranges for the human body. Mixing of elemental powders was carried out in a 2 L Inversin BioEngineering mixer at 50 rev min^{-1} for 45 min. Mechanical mixing was performed in a planetary mill (Retsch PM400/2) running at 180 rev min^{-1} for 52 min in chrome steel jars. The ball-to-powder ratio used for the milling process was 10:1 under argon atmosphere. After milling, the powders were dried under vacuum and compacted uniaxially in a matrix of 30 × 12 × 5 mm geometry at 100 MPa. The sintering was carried out in a high vacuum tube furnace Carbolite HVT 15-75-450 at 0.05 Pa. Before sintering, the furnace chamber was filled with argon and evacuated twice. The sintering was executed in two cycles: 1) Heating up to 780 °C at a rate of 10 °C min^{-1} and holding temperature for 60 min, and b) Heating up to 1300 °C at a rate of 7 °C min^{-1} and holding for 180 min with posterior furnace cooling.

2.2. Microstructural characterization

Before microstructural characterization, the samples were subjected to conventional metallographic grinding and polishing up to mirror appearance with 9 μm diamond suspension followed by 0.04 μm colloidal silica diluted with 10 vol% hydrogen peroxide. The samples were cleaned with distilled water and ethyl alcohol/acetone for 15 min in an ultrasonic bath.

The identification and quantification of phases was performed by X-ray diffraction (Bruker/D2Phaser) with Cu Kα radiation (λ = 0.15418 nm) at 30 kV and 10 mA, step of 0.02° and scanning speed of 0.0025° s^{-1}. Refinement of the structural parameters and the quantitative analysis of the phases were

carried out by MAUD software (version 2.94). The porosity, phases distribution and morphology were observed by the difference in contrast through optical microscopy (Nikon Eclipse LV100DA) and field emission scanning electron microscopy (FESEM, ZEISS-ULTRA 55) with an energy dispersive X-ray spectroscopy (EDS) detector. An electron backscatter diffraction detector (EBSD, Oxford Instruments Ltda.) coupled to the FESEM was used to analyze the crystallographic texture. The density and porosity were investigated by the Archimedes method according to the ASTM B328 standard.

2.3. Mechanical behavior

Microhardness was obtained with a Shimadzu HMV tester applying a load of 1.9 N for 10 s. At least 5 hardness measurements were obtained. Flexural strength was determined by a four-point flexural test on samples with a geometry of 28 × 11 × 5 mm at room temperature at a constant speed of 0.5 mm min^{-1}, employing a Shimadzu Autograph of 100 kN. The space between down supports was 22 mm and upper supports was 11 mm with a relation 1/2. A dynamic technique was used instead of mechanical methods to secure a higher precision and repeatability of elastic modulus measurement [38]. The elastic modulus, E, was evaluated using the impulse excitation technique (ATCP, Sonelastic). The software ATCP Sonelastic 3.0 was used to analyze the data. Three measurements of flexion and five of elastic modulus were taken for statistical purposes.

2.4. Ion release and electrochemical evaluations

For ion release evaluation, the samples were embedded in methacrylate and the borders were sealed with transparent enamel to delimit the exposed area of 1.12 cm^2. Subsequently, the samples were subjected to direct contact with 50 mL of modified Ringer-Hartmann artificial saliva with a pH of 6.5 ± 0.2 (5.97 NaCl, 0.37 KCl, 0.22 $CaCl_2$, and 3.25$C_3H_5O_{3x}Na$ g L^{-1}) in sterile bottles. The samples were kept at the average body core temperature, i.e., 37 °C [39], for 730 h. After incubation, the morphology of samples was studied under optical and scanning electron microscopes. Inductively coupled plasma optical emission spectrometry (ICP-OES, Varian-715ES) was used to measure the concentrations of Ti, Nb, and In ions dissolved in the incubated medium. Three samples were analyzed for statistical purposes.

The corrosion study was carried out by a potentiostat/galvanostat (Metrohm potentiostat-PGSTAT204) on an exposed surface of 0.785 cm^2 using a three-electrode cell in the previously mentioned modified Ringer-Hartmann solution at 37 °C. Ag/AgCl and platinum electrodes were used as a reference and auxiliary electrodes, respectively. The open circuit potential (OCP) measurements were performed for 2 h. The electrochemical impedance spectroscopy (EIS) analyses were performed with a sinusoidal perturbation of 10 mV amplitude and a frequency sweep from 100 to 5 kHz was applied. The frequency response was analyzed using ZView software. The corrosion parameters were determined by Tafel's extrapolation methods using Wolfram Mathematica 12.1 software. The measured density of the Ti–35Nb–5In alloy (5.03 g cm^{-3}) was considered to estimate the corrosion rate. The curves were plotted in OriginPro 8.5 software, and three samples per condition were studied.

3. Results and discussion

3.1. Microstructural characterization

From Fig. 1a–d, the Ti–35Nb–5In alloy obtained from the P&S method showed heterogeneous dispersion of alloying elements through the microstructure. As shown in Fig. 1d–f, Nb was segregated through the microstructure. From the binary Ti–In and Ti–Nb diagram phases, a melting point ≤1800 °C can be expected for the Ti–35Nb–5In [40,41]. Due to the small particle size of powders, sintering temperatures from 70 to 90% of the melting point of the bulk alloy are preferred during sintering [16]. Thus, the sintering temperature of 1300 °C was expected to be high enough to allow atomic diffusion through the microstructure. Similar Nb immiscible zones were obtained in a hot P&S Ti-40 wt% Nb alloy [42]. The Nb segregation might be related to the low Nb solubility in the α-Ti phase [40], which was formed during cooling. This was also observed in P&S Ti–Nb alloys with a lower Nb content in the α phase compared to the β one [42]. However, particle size distribution and morphology, surface texture, density, or cohesivity could also affect the Nb diffusion during sintering or cooling [43].

Fig. 1a shows micrometric grain sizes in the Ti–35Nb–5In that are highly similar to those obtained in cast Ti–36Nb and Ti–40Nb alloys [44]. Micropores are also frequent in the micrograph. By the Archimedes method, the relative density of the Ti–35Nb–5In alloy was 92.83 ± 0.19%, which agrees well with the micrograph from Fig. 1a. Porosities as low as the obtained in this alloy can be considered mainly as closed porosity [45].

Fig. 2 shows the phase content studied by XRD and EBSD techniques. The Ti–35Nb–5In alloy was mainly composed by BCC β-Ti phase (83.3%), as well as HCP α (9.5%) and orthorhombic α'' (7.2%) in lower percentages. Other phases, such as α', were not identified by XRD in the Ti–35Nb–5In alloy, which may be related to their non-existence (associated to the high Nb content [46]) or to a low volume fraction below the detection range.

The obtained 83.3% of β phase was congruent with the β-rich microstructures in P&S Ti–40Nb [42], cast Ti–40Nb and Ti–40Nb–4In Ref. [34], and cast Ti with 30–40 mass% of Nb [44] from the literature. However, the fabricated alloy also contains 5 wt% of In, which can form a solid solution with Ti up to contents of about 20 wt% [47]. It has been reported that Ti alloys with 2.5–10 wt% of In tend to form single α phase microstructures. It should be mentioned that there is no general agreement regarding the In effect on the formation of β-Ti and α-Ti [4] phases. Some works hypothesized a probable β-Ti stabilization by lowering its critical transformation temperature with In additions [41]. Although, the scarce reported Ti–In alloys were single α-Ti phase up to ~44 wt% In obtained by arc-melting [41,47] and up to 10 wt% In obtained by powder metallurgy [23].

From Fig. 2b–e, the microstructure is composed of acicular α and fine α'' phases inside nearly equiaxed and micrometric β phase. From Fig. 2c–d, the α phase is mainly found at the β

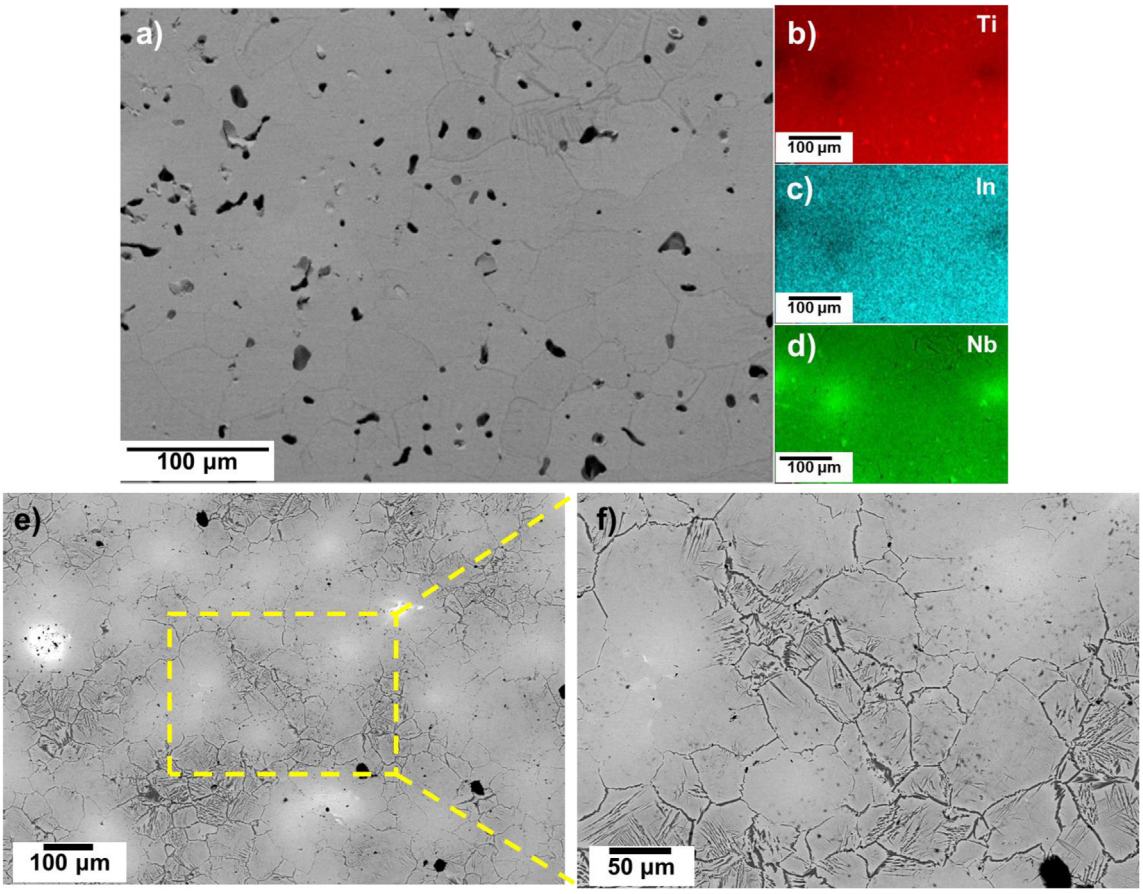

Fig. 1 – (a) Micrograph showing porosity, (b–d) EDS mappings of constituent elements, and (e–f) grains morphology of the of the Ti–35Nb–5In alloy.

boundaries. The preferred precipitation of α phase at the β boundaries is a common phenomenon explained by the well-known high energy at triple junctions as first precipitation sites, subsequent growing along β boundaries, and posterior growing at the inner grain space [48]. On the other hand, the α'' used to form fine structures within the α acicular plates, which was also observed in the Ti–35Nb–5In alloy.

The α'' is an intermediate phase during the β (BCC) to α (HCP) transformation [49], and it requires smaller strains to form compared to the required for the equilibrium α phase. Such strains can be applied by non-equilibrium cooling or mechanically. The second one could be the case of the present Ti–35Nb–5In alloy. The deformation-induced α′-martensite could be triggered in the β matrix by the compressive stress applied to the powders during compaction at room temperature. The transformation of α′ to α could be later promoted during sintering. However, the high quantity of Nb β-stabilizer in the Ti–35Nb–5In alloy could promote the formation of intermediate metastable α'' [46]. As a result, the microstructure retained a minor percentage of α'' that is shown in Fig. 2a. Parallelly, the high β-stabilizers content restricted the α formation.

Fig. 2f shows the experimental correlated (green bars) and uncorrelated (orange bars) misorientation histograms for the dominant β phase in the Ti–35Nb–5In alloy. The theoretical uncorrelated (gray profiles) misorientation profiles for randomly oriented cubic crystals was also included for comparison. Due to the uncorrelated misorientation profiles were obtained between random points that are not necessarily contiguous at the microstructure, it includes the effect of transgranular misorientation. Complementarily, the correlated misorientation represents the angle comparisons between adjacent points that, from statistics, frequently belong to the same grain.

From Fig. 2f, the uncorrelated misorientation histogram of the β phase followed a similar tendency to the theoretical random texture distributions. Thus, the β phase grew under a nearly random crystallographic orientation. However, as the correlated and uncorrelated profiles between β and α phases are highly different, they suggest differences between the misorientations at the inner grain and their neighborhood [50]. From the above, the grains are not free of substructures and possible transgranular strain, which could be caused by the dispersed fine α'' phase (Fig. 2e). Besides, the α'' frequently involves twinning generated during the transformation strain from the β phase [51,52].

As the α and α'' phases have irregular shapes, the grain length instead of grain diameter distributions was obtained from EBSD measurements as shown in Fig. 3. The 100% and 90% of the total grains of α'' and α phases are below grain lengths of 20 μm. The β phase has a visibly broader grain length distribution. The small size of the metastable α'' and α phases agrees with the

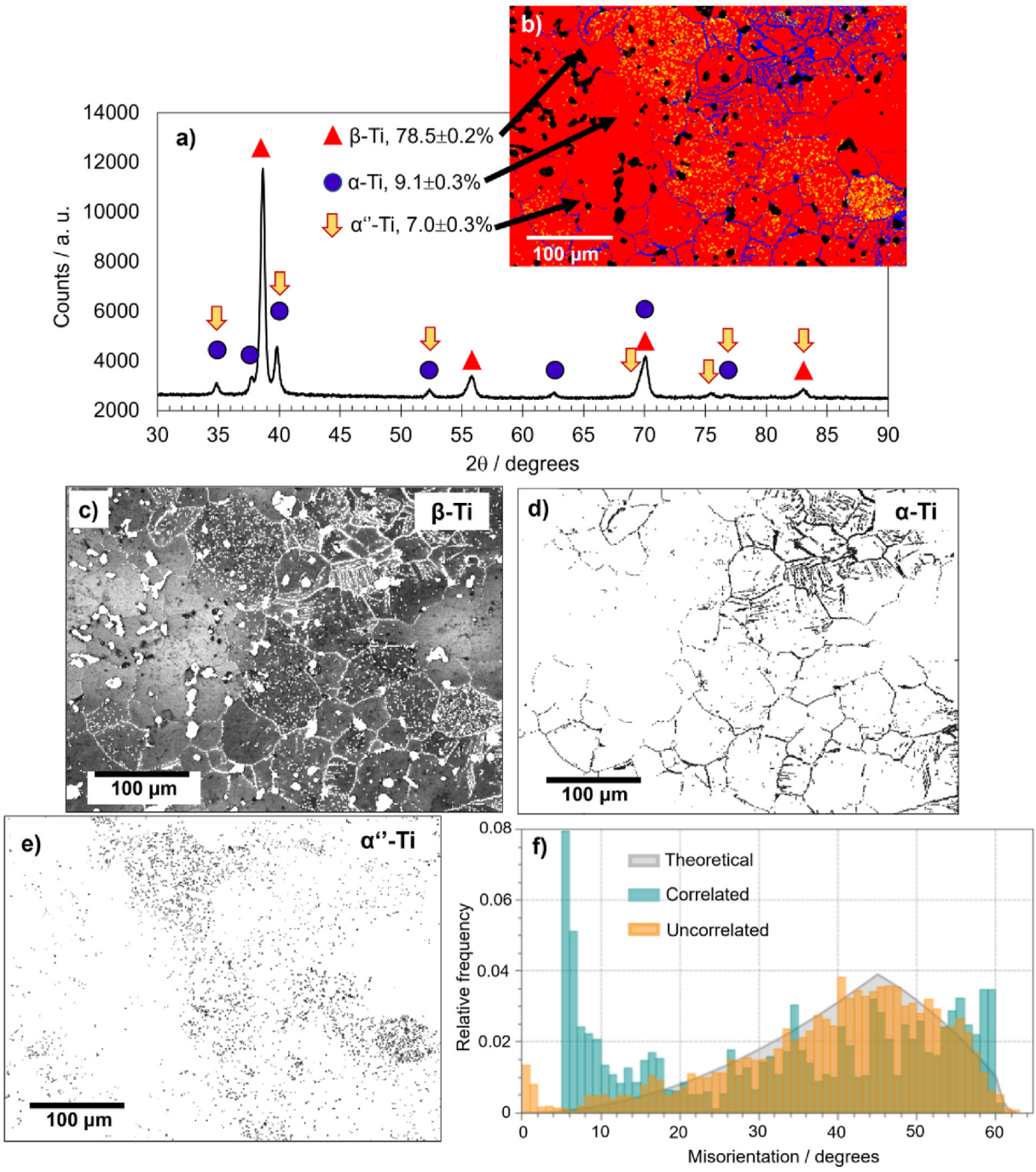

Fig. 2 – Phases analyses on the Ti–35Nb–5In alloy. (a) Diffractogram and (b) EBSD micrograph contrasting the β, α, and α'' phases by red, blue, and yellow colors, respectively, (c–e) EBSD micrographs showing the phases distribution in more detail, and (f) and comparison of theoretical (random) uncorrelated and experimental correlated and uncorrelated misorientation profiles for the most abundant phase (β).

solidification stages that start by β phase. Furthermore, grain growth pinning effect due to In additions was reported in P&S-obtained Ti–5In alloy [23]. However, the reported pinning effect of In was attributed to the segregations at the grain boundary, which were not observed in the present work. The segregations of Nb observed in Fig. 1 might restrict the grain growth of the Ti alloy due to the decreased mobility of the grain boundary through the dragging effect.

3.2. *Mechanical behavior*

To study the mechanical performance of the new Ti–35Nb–5In alloy during flexural and compressive stress, e.g., during the impact of the upper and lower teeth due to chewing or joint flexions, four-point flexural and microhardness tests were carried out. The results from the five flexural repetitions are shown in Fig. 4a. All the repetitions showed

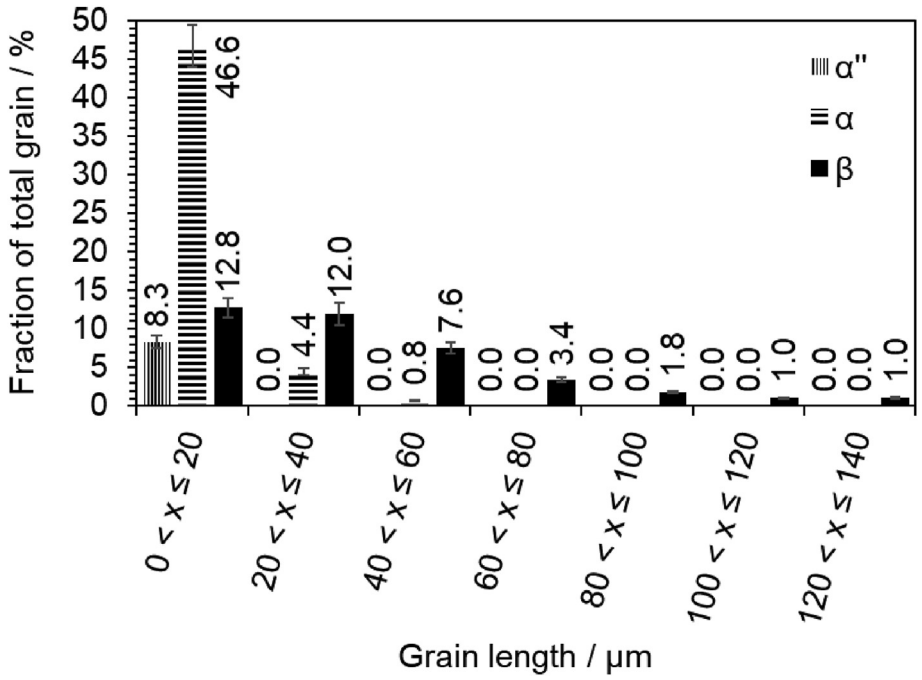

Fig. 3 – Grain length distribution with respect to a total of 484 analyzed grains on the Ti–35Nb–5In alloy.

good reproducibility, which translated to acceptable errors and reliability of results.

For orthopedic applications, the mechanical behavior of the Ti–35Nb–5In alloy should be compared to that of the human bone, as well as the other reported Ti alloys for biomedical applications. The flexural strength of the Ti–35Nb–5In alloy (0.61 GPa) is higher than the bending strength of the human bone (0.35 and 0.39 GPa) [53]. Besides, the flexural strength of the Ti–35Nb–5In alloy is also higher than the bending strength reported for binary Ti–In alloys (~0.3 GPa) [23] and mechanically mixed Ti–Zr alloys (0.47–0.50 GPa) [54].

Low elastic moduli, near the one of human bone, are essential to reduce the mechanical mismatch between bone and implant, decreasing the implant failure rate. The mechanical mismatch promotes bone stress shielding and bone tissue degradation [55]. The elastic modulus of the Ti–35Nb–5In alloy (63 GPa) was higher than the reported for human femur bone (<25 GPa [56]), but lower than several Ti alloys that have been reported as feasible for orthopedic purposes. Examples of the above are Ti–In (114–117 GPa) [23] and Ti–Zr alloys (82–115 GPa) [54].

The low elastic modulus of the Ti–35Nb–5In alloy was compared with other low-porosity Ti-based implant alloys in Fig. 4b. The higher content of β phase in the Ti–35Nb–5In alloy can be related to its lower elastic modulus compared to Ti–In, and Ti–Zr alloys (mostly constituted by α phase). It is widely reported that the β-Ti alloys possess lower elastic modulus than the α phase [25]. The elastic modulus of the Ti–35Nb–5In alloy (63 GPa) was nearer to the reported β-like Ti–Nb–Mo alloys (64–96 GPa) [57] and down from the Ti–35Nb alloy (94 GPa) [58]. Considering that the 5 wt% In might promote a higher elastic modulus [23], the lower elastic modulus of the Ti–35Nb–5In compared to the Ti–35Nb alloy might be related to the porosity. The reported Ti–35Nb has no porosity [58], while the Ti–35Nb–5In from this work has a relative density of 92.8%.

The hardness of the Ti–35Nb–5In alloy (~2.7 GPa) was up to the hardness reported for osteonal, interstitial, and trabecular bone regions (0.23–0.76 GPa) [56]. Besides, it was comparable to that of multiple Ti alloys designed for orthopedic purposes, such as Ti–6Al–4V (~2.8 GPa) [59], Ti–In (1.3–1.4 GPa) [23], and Ti–Nb–Mo alloys (1.8–2.8 GPa) [57].

The hardness of the Ti–35Nb–5In alloy can be related to its chemical composition that promotes the formation of different phases. From the literature, Ti–In and Ti–Nb alloys with 5 wt% In and 35 wt% Nb contents have lower (~1.4 GPa [23]) and higher (~3.1 GPa [58]) hardness than the Ti–35Nb–5In alloy (~2.7 GPa), respectively. While the In promoted a single-α phase microstructure, the Nb promoted a nearly β phase microstructure when cooled at equilibrium. Thus, the hardness of the 83.3% β (Fig. 2a) Ti–35Nb–5In alloy is congruent with the higher hardness of nearly-β Ti–35Nb alloy [58] and the lower hardness of single-α Ti–5In alloy [23] from the literature.

The grain size and porosity might not significantly influence the hardness of the compared alloys. The grain size of the dominant β phase in the Ti–35Nb–5In alloy (5–125 μm) is smaller than that of the dominant α phase in Ti–5In (50–150 μm [23]) and the β phase in Ti–35Nb (280 μm [58]) alloys. Despite the above, the hardness of the Ti–35Nb–5In is between that of the Ti–5In and Ti–35Nb alloys. Furthermore, the relative density in the three compared alloys is at least 92.8%.

From the above, the good mechanical properties of the Ti–35Nb–5In alloy might be mainly related to its chemical composition and the promoted phases content. Besides, the Ti–35Nb–5In alloy showed a good agreement with the mechanical properties of several reported implant materials, including the Ti–5In and Ti–35Nb alloys [23,58]. Thus, the Ti–35Nb–5In alloy meets the mechanical requirements for its use in orthopedic applications.

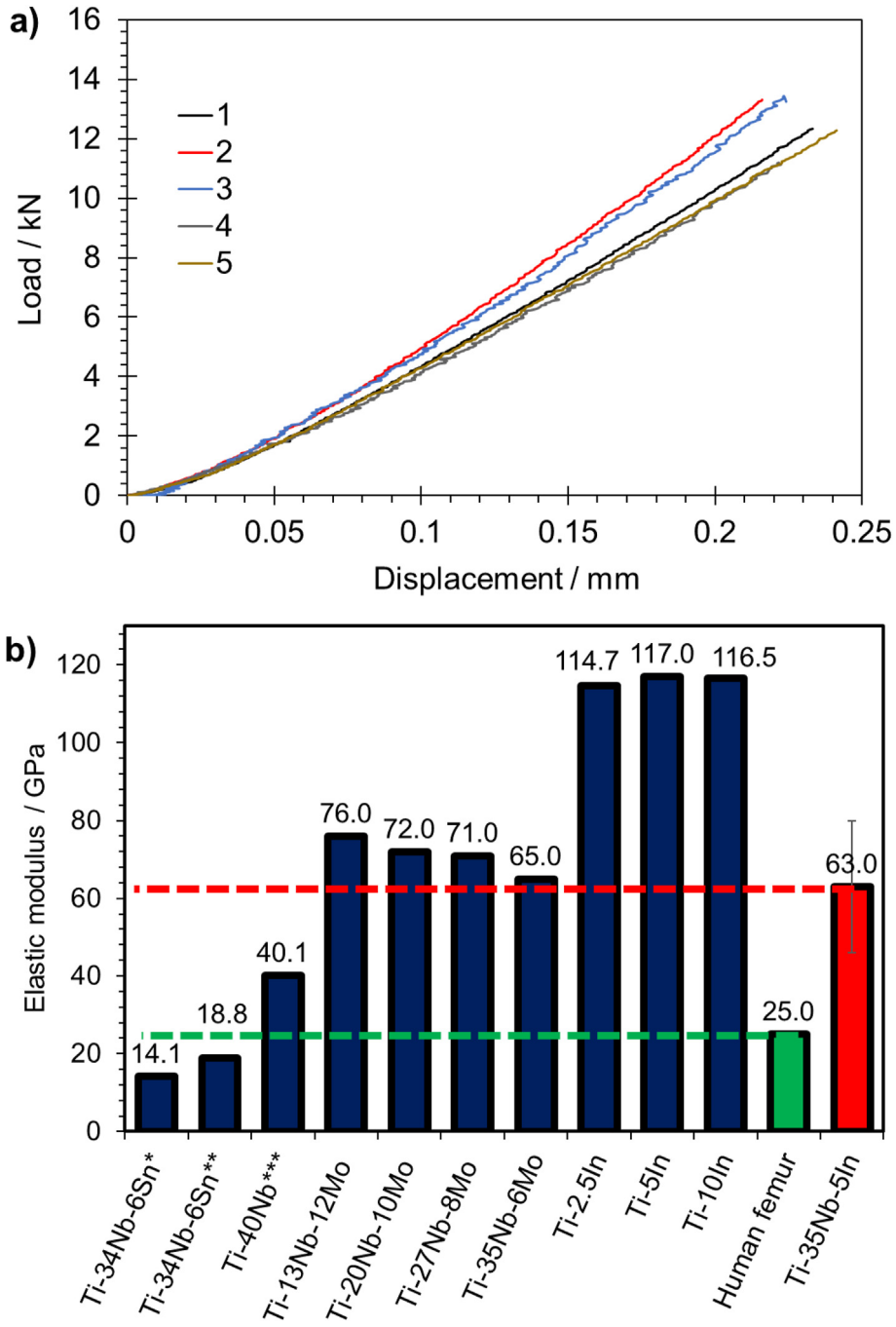

Fig. 4 – (a) Four-point flexural results of the Ti–35Nb–5In alloy and (b) comparison of the elastic modulus of the Ti–35Nb–5In of this work (red dotted line) with the human femur (green dotted line) and other low-porosity (relative density >93%) alloys from the literature obtained by P&S [20,23,57]. *, **, * refer to compaction pressure of 100 MPa and 200 MPa, and 1-h sintering at 1200 °C, respectively.**

3.3. *Ion release and electrochemical evaluations*

Metal ion release rates are crucial to ensure the low toxicity of biomaterials with potential applications for oral devices. A safe oral implant material should demonstrate metallic ion release rates below the recommended dietary intake or reported toxicity levels.

From Table 1, the ion release of the three constituent elements was below the harmful levels for the human body. The Ti^{3+} concentration was well below the limits of 10 ppm (10,000 $\mu g\ L^{-1}$) and 5 ppm (5,000 $\mu g\ L^{-1}$), which inhibit and do not stimulate cell proliferation, respectively [60]. Moreover, the In release was well below the limit of 2310 μM ($2.65 \times 10^5\ \mu g\ L^{-1}$), which caused 50% L-929 fibroblast death

Table 1 – Average metallic ion release and corrosion rate from the Ti–35Nb–5In alloy when tested in modified Ringer-Hartmann artificial saliva.

Ion release rate ($\mu g\ L^{-1}\ cm^{-2}\ h^{-1}$)			Corrosion rate ($mg\ dm^{-2}\ day^{-1}$)	Corrosion rate ($\mu m\ year^{-1}$)
Ti	Nb	In		
0.019 ± 0.007	0.022 ± 0.005	0.004 ± 0.003	0.005 ± 0.001	0.070 ± 0.020

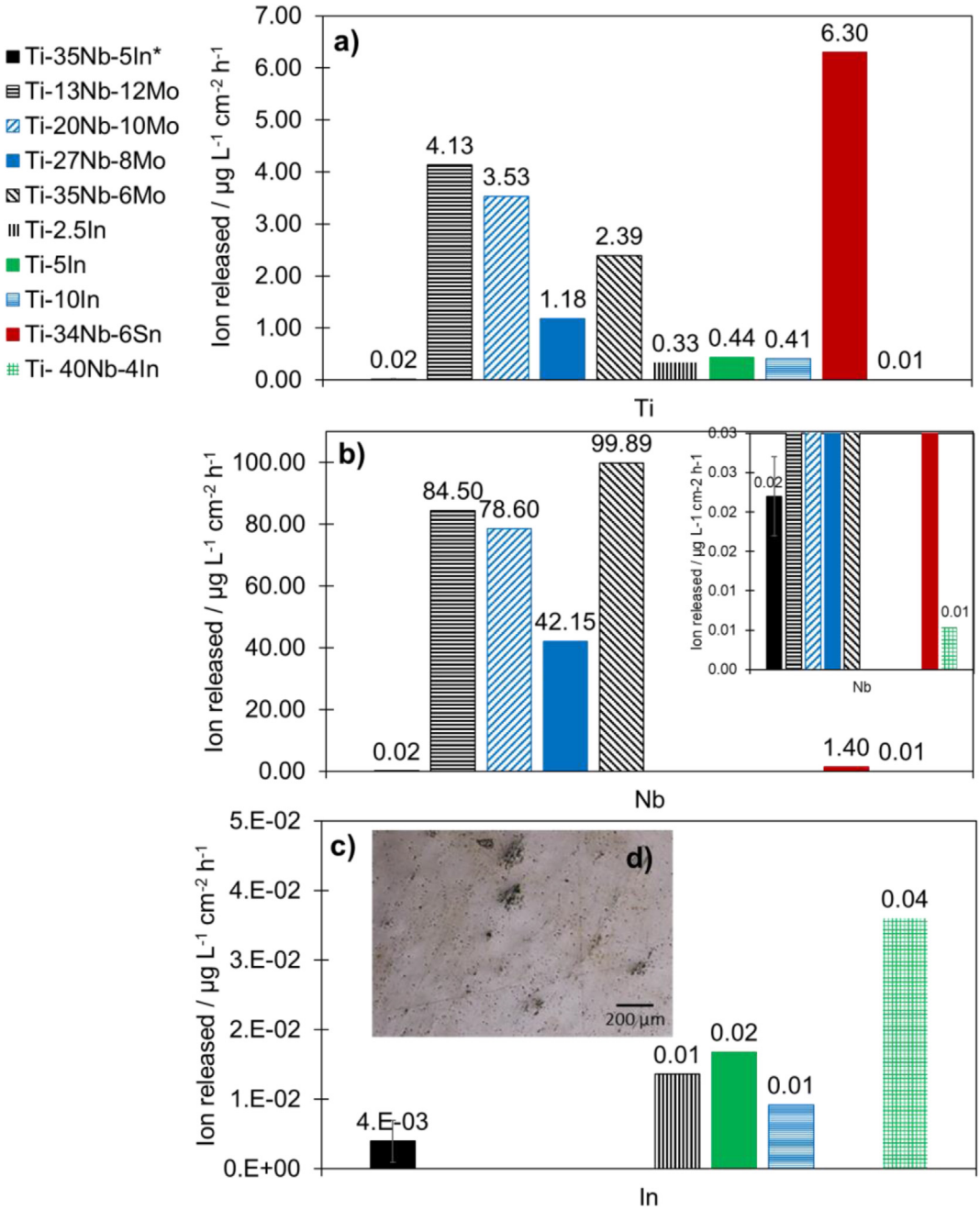

Fig. 5 – Comparison of (a) Ti, (b) Nb, and (c) In ion release among different low-porosity Ti–35Nb–5In (*this work), P&S Ti-In Ref. [23], P&S and laser surface treatment at 1000 W Ti-Nb-Mo [57], of P&S at 100 MPa Ti-Nb-Sn [20], and cast Ti-Nb-In Ref. [34] alloys. The alloys were tested in Fusayama artificial saliva (pH from 5.2 to 5.8) [20,23,57], buffered saline solution (pH = 7.6) [34], or modified Ringer-Hartmann artificial saliva for the alloy of the present work (pH = 6.5). (d) Micrograph of the Ti–35Nb–5In alloy after ion release testing.

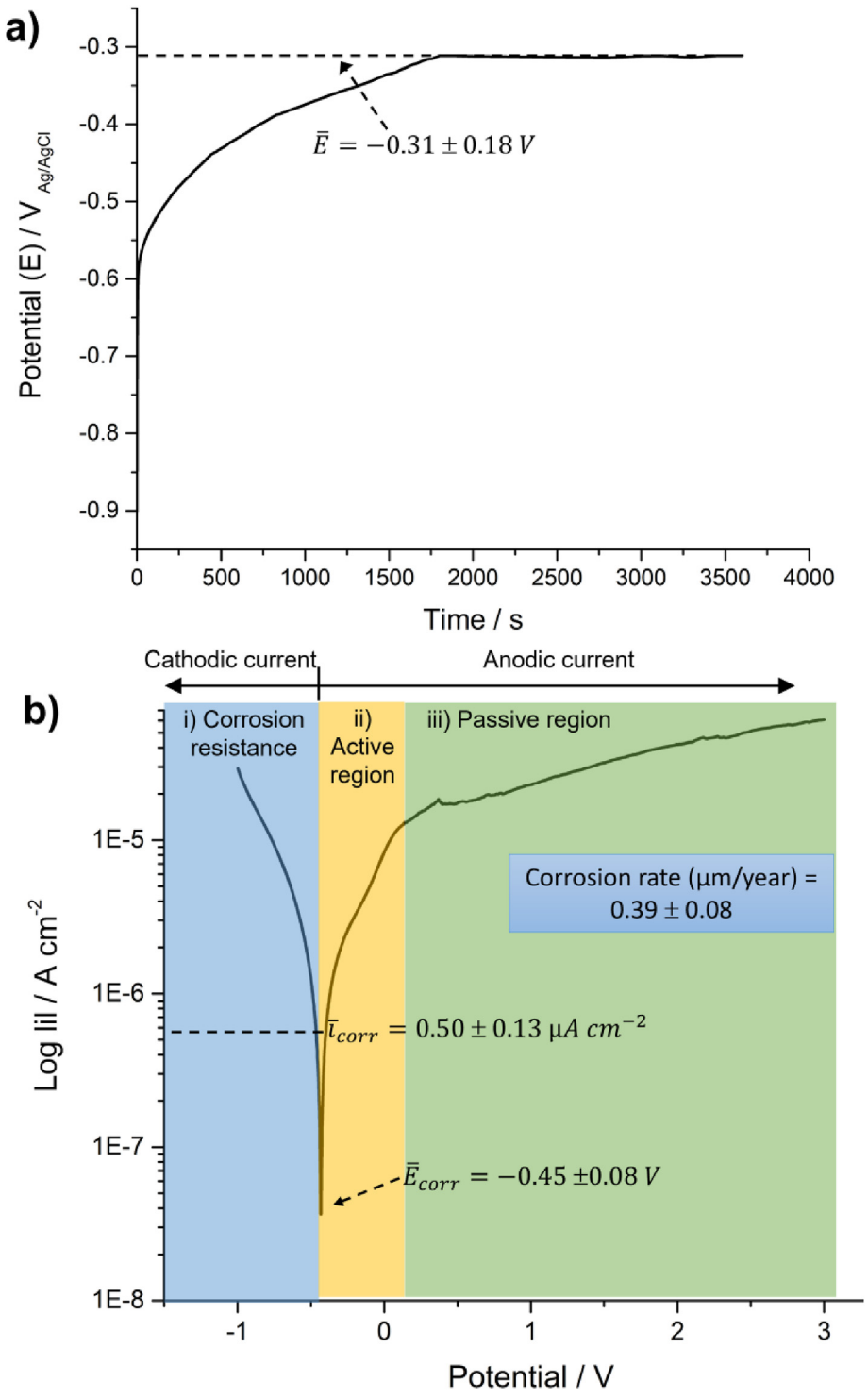

Fig. 6 – (a) OCP and (b) PD polarization curves for the Ti–35Nb–5In alloy measured at modified Ringer-Hartmann artificial saliva.

[61]. Another report pointed out that In is non-toxic below 50 ppm (50,000 μg L^{-1}) [62], which is also quite up to the ion In^{3+} release measured in this work. Regarding Nb, the ion release up to 0.022 μg L^{-1} cm^{-2} h^{-1} (6.4 × 10^{-6} mM day^{-1}) is below the 0.5 mM of Nb^{5+} that induced <50% viability, i.e., concentration at which 50% of the cells were viable [63]. The Nb release from the Ti–35Nb–5In alloy is also below the non-toxic concentration of 172.0 μg/L [30]. From the above, the ion release rates from the Ti–35Nb–5In alloy met the non-toxicity requirement for its use as biomedical implants.

Considering that this is the first report of the Ti–35Nb–5In alloy, comparisons with other low-porosity (relative density

>93%) Ti alloys from the literature were made. Fig. 5 allows evaluation of the advantages of the Ti–35Nb–5In alloy for biomedical purposes. The Ti–35Nb–5In alloy released lower concentrations of Ti, Nb, and In (Fig. 5a–c) compared to the Ti-Nb-Mo [57], Ti-In Ref. [23], and Ti–Nb–Sn [20] systems. However, compared to the dense (cast) Ti–40Nb–4In alloy from the literature [34], the P&S Ti–35Nb–5In alloy released more Ti and Nb. This ion release difference could be related to the different bonding strengths obtained from the different processing routes and testing conditions. Comparisons between porous and dense alloys have shown higher ion release from the former [59]. Furthermore, the Ti–40Nb–4In from the literature was tested in a less aggressive environment of tris-buffered saline (TBS) solution with pH = 7.6, compared to that of the present work of Ringer-Hartmann solution with pH = 6.5.

Among the factors influencing the corrosion resistance of P&S-elaborated alloys are the chemical composition and heterogeneities, porosity, grain size, and phase content. Regarding chemical composition and heterogeneities, In has improved the corrosion resistance of multiple alloys [64], including Ti [23]. The average corrosion rate of the Ti–35Nb–5In alloy of 0.005 mg dm^{-2} day^{-1} (Table 1) is similar to that of Ti–In alloys and commercially pure Ti (CP–Ti) [47].

Niobium, on the contrary, showed a preferred degradation in the corrosive media. The localized corrosion of the Ti–35Nb–5In alloy (Fig. 5d) may be related to the Nb segregations shown in Fig. 1. The tendency of preferred attack at the Nb segregation regions is also congruent with the higher Nb release compared to Ti and In the Ti–35Nb–5In alloy. A similar preferred attack of Nb was reported in Ti–Nb–Mo alloys [57]. Thus, In and Nb might promote different corrosion tendencies in the Ti–35Nb–5In alloy. Systematic electrochemical studies are necessary to describe the effect of chemical composition, grain size, and phase percentage on the corrosion rate after artificial saliva immersion.

Regarding grain size, the high density of grain boundaries allows a more compacted and well-adhered surface passive layer in Ti alloys compared to coarse grained alloys [65]. The new Ti–35Nb–5In alloy has a 68% of grain sizes below 20 μm (Fig. 3). However, the Ti–35Nb–5In alloy showed a lower corrosion rate (0.005 mg dm^{-2} day^{-1}) than a reported Ti–35Nb–6Mo processed at beam power of 1000 W (12.32 mg dm^{-2} day^{-1}) with an average grain size of 16.21 μm [57]. Thus, among the factors influencing the corrosion behavior, the grain size might not be dominant in the Ti–35Nb–5In alloy.

The good corrosion resistance of the Ti–35Nb–5In alloy could also be related to the phase percentage. The α/β interfaces are preferably attacked when immersed in HCl and artificial saliva media (without electric current applied) [59,66]. Thus, higher corrosion resistance is expected in single-phase Ti alloys. However, the tri-phasic microstructure of the Ti–35Nb–5In alloy showed a lower corrosion rate in artificial saliva than other reported near single α and β phases Ti alloys [23,57]. Thus, the phase content might not be a determining factor for the corrosion behavior of the

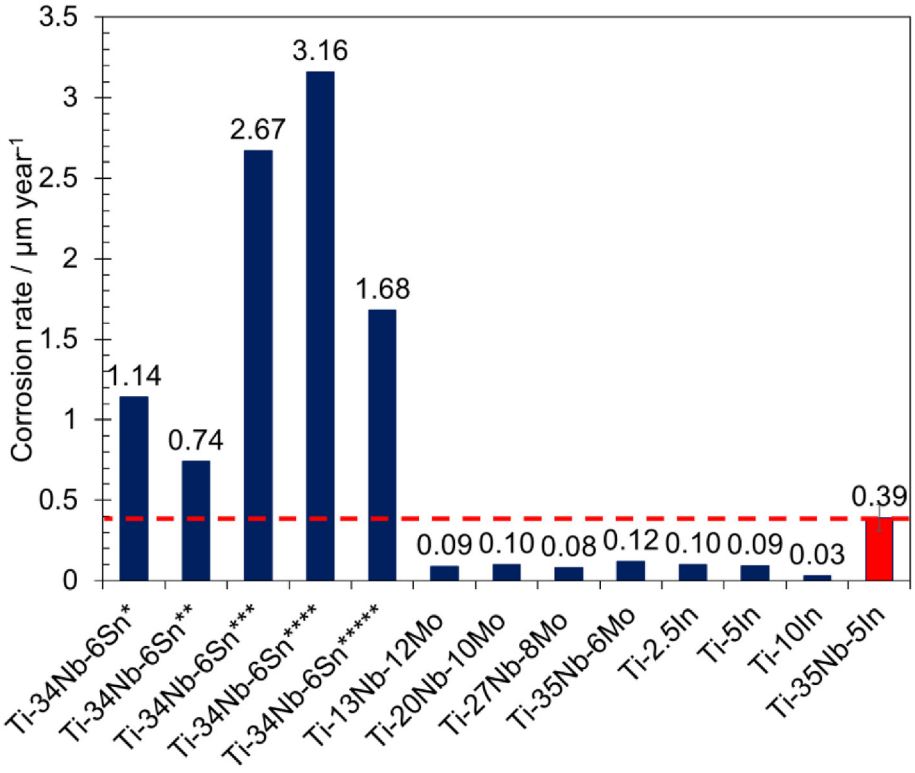

Fig. 7 – Comparison of corrosion rate among the Ti–35Nb–5In of this work (red dotted line) and other Ti-alloys produced by P&S [20,23,57] and electrical resistance sintering (ERS) [68] tested in Fusayama artificial saliva [20,23,57] or Ringer-Hartmann solution ([68] and this work). *, **, *, ****, and ***** refers to P&S at 100 MPa and 200 MPa [20], and ERS at 11, 12, and 13 kA [68], respectively.**

Ti–35Nb–5In alloy. From the above, the chemical inhomogeneities and the porosity might be the key factors that govern the corrosion performance of the Ti–35Nb–5In alloy.

The electrochemical behavior of the Ti–35Nb–5In alloy in Ringer-Hartmann solution is shown in Fig. 6. The corrosion parameters shown in the graphs correspond to the average between the three measurements. From the low porosity of the Ti–35Nb–5In alloy (7.2%), the contact area considered for the corrosion calculations corresponded to the surface of the sample (0.785 cm^2) assuming it as a dense material. As the surface area of low-porosity Ti–Nb alloys has been shown as non-relevant for the corrosion performance [67], the pores surface area was not considered on the corrosion calculations.

Fig. 6a presents the open circuit potential (OCP) graph. The OCP values are negative (average of −0.31 ± 0.18 V), indicating that the ground base alloy was active. The corrosion potential increased in the primary immersion stage up to times <1780 s; then, it remained almost constant. The stabilization of OCP values indicates the surface passive layer formation. It is noteworthy that higher OCP values at the steady-state were obtained compared to P&S at 200 MPa Ti–34Nb–6Sn (−0.47 V) [20], dense Ti–6Al–4V ELI, Ti–13Mo–7Zr–3Fe (TMZF), and Ti–35Nb–7Zr–5Ta (~-0.33 to −0.36 V) [66] alloys, implying the formation of a more stable surface oxide layer. Besides, the OCP of the Ti–35Nb–5In alloy showed a similar passivation behavior to the P&S Ti–5In (−0.32 V) [23] and additively manufactured Ti–6Al–4V (−0.31 V) [59] alloys.

Fig. 6b shows the potentiodynamic (PD) polarization curves of the Ti–35Nb–5In alloy. The alloy exhibited an electrochemical behavior described by; i) corrosion resistance region, where the cathodic behavior takes place, ii) active general corrosion region and starting of the anodic behavior, and iii) formation of surface oxide passive film. The less negative E_{corr} of the Ti–35Nb–5In (−0.45 V) compared to that of other P&S Ti–34Nb–6Sn alloys (−0.5 to −0.72 V) indicates a lower electrochemical activity of the former. This might be related to forming a more stable surface oxide film in the Ti–35Nb–5In.

For a more detailed comparison, the corrosion rate of the Ti–35Nb–5In alloy was estimated at a value of 0.39 μm $year^{-1}$. Its corrosion rate was compared to other implant Ti alloys in Fig. 7. The Ti–35Nb–5In alloy showed superior electrochemical performance compared to the Ti–Nb–Sn system obtained by P&S and ERS [20,68], but inferior to the P&S Ti–Nb–Mo and Ti–In alloys [23,57]. As seen in Fig. 5, corrosion occurrence preferred Nb segregation regions over the In-enriched grains. Besides, the reported Ti–Nb–Mo had a laser surface treatment that significantly improved their corrosion resistance [57].

From the above, it has been shown that the Ti–35Nb–5In alloy has an acceptable electrochemical performance compared to several Ti alloys designed for implant purposes. Moreover, the corrosion rate of 0.39 μm $year^{-1}$ allows considering the Ti–35Nb–5In as perfectly stable [69]. The good corrosion resistance of the Ti–35Nb–5In alloy suggests adequate biocompatibility and osteointegration [70], which are critical factors for the effectivity of metallic alloys as biomedical implants.

4. Conclusions

This is the first report of an alloy of the Ti–Nb–In system with a porous microstructure. The mechanical properties, toxicity, and electrochemical assessment uncovered the porous Ti–35Nb–5In alloy as a feasible candidate for biomedical implant applications. This conclusion was based on the following specific findings:

(1) The microstructure of the Ti–35Nb–5In alloy consisted of acicular α and fine dispersed α'' phases within a nearly-equiaxed and micrometric β phase matrix. The correlated and uncorrelated misorientation profiles suggested random crystallographic texture on the β matrix.
(2) The elastic modulus of the Ti–35Nb–5In alloy was 2.5 times higher (63 GPa) than the reported for the human femur but smaller than other reported implant Ti alloys. The hardness (2.7 GPa) and flexural strength (0.61 GPa) were higher than those reported for the human bone.
(3) The Ti, Nb, and In releases (Ti: 0.019; Nb: 0.022; and In: 0.004 $\mu g L^{-1}$ cm^{-2} h^{-1}) were below toxic levels for the human body. The corrosion rate (0.39 μm $year^{-1}$) was below several reported implant materials. In general, the corrosion performance was mainly influenced by chemical inhomogeneities (preferred dissolution of Nb segregates) and porosity.

Data availability

The raw data related to this manuscript would be made available on request.

Declaration of competing interest

The authors declare that they have no known competing financial interests or personal relationships that could have appeared to influence the work reported in this paper.

Acknowledgments

This work was made possible with funding support from various sources. VAB acknowledges the funding from the Spanish Ministerio de Ciencia, innovación y Universidades with research project RTI2018-097810-B-I00, and the European Commission via FEDER funds, which allowed to purchase research equipment and the Microscopy Service at the Universitat Politècnica de València. MCR thanks the Fundação de Amparo à Pesquisa do Estado de São Paulo for financial support to carry out this work with "Projeto Temático" nº 2018/18293–8 and post-doc Grant Nos. 2018/18293–8 and 2021/03865–9.

REFERENCES

[1] Klug A, Gramlich Y, Rudert M, Drees P, Hoffmann R, Weißenberger M, et al. The projected volume of primary and revision total knee arthroplasty will place an immense burden on future health care systems over the next 30 years. Knee Surg Sports Traumatol Arthrosc 2021;29:3287–98. https://doi.org/10.1007/s00167-020-06154-7.

[2] Kurtz S, Ong K, Lau E, Mowat F, Halpern M. Projections of primary and revision hip and knee arthroplasty in the United States from 2005 to 2030. J Bone Jt Surg - Ser A 2007;89:780–5. https://doi.org/10.2106/JBJS.F.00222.

[3] Elani HW, Starr JR, Da Silva JD, Gallucci GO. Trends in dental implant use in the U.S., 1999–2016, and projections to 2026. J Dent Res 2018;97:1424–30. https://doi.org/10.1177/0022034518792567.

[4] Chen L, Cui Y, Zhang L. Recent development in beta titanium alloys for biomedical applications. Metals 2020;10:1139.

[5] Yılmaz E, Kabataş F, Gökçe A, Fındık F. Production and characterization of a bone-like porous Ti/Ti-hydroxyapatite functionally graded material. J Mater Eng Perform 2020;29:6455–67. https://doi.org/10.1007/s11665-020-05165-2.

[6] Geetha M, Singh AK, Asokamani R, Gogia AK. Ti based biomaterials, the ultimate choice for orthopaedic implants - a review. Prog Mater Sci 2009;54:397–425. https://doi.org/10.1016/j.pmatsci.2008.06.004.

[7] Gratton A, Buford B, Goswami T, Gaddy Kurten D, Suva L. Failure modes of biomedical implants. J Mech Behav Mater 2011;13:297–314. https://doi.org/10.1515/jmbm.2002.13.5-6.297.

[8] Goia TS, Violin KB, Yoshimoto M, Bressiani JC, Bressiani AHA. Osseointegration of titanium alloy macroporous implants obtained by PM with addition of gelatin. Adv Sci Technol 2010;76:259–63. https://doi.org/10.4028/www.scientific.net/ast.76.259.

[9] Bram M, Ebel T, Wolff M, Barbosa APC, Tuncer N. Applications of powder metallurgy in biomaterials. Adv Powder Metall 2013;520–54. https://doi.org/10.1533/9780857098900.4.520.

[10] Xu Wei, Lu Xin, Zhang Bing, Liu Chengcheng, Lv Shaomin, Yang Shidi, Xq. Effects of porosity on mechanical properties and corrosion resistances of PM-fabricated porous Ti-10Mo alloy. Metals 2018;8:188. https://doi.org/10.3390/met8030188.

[11] Pałka K, Pokrowiecki R. Porous titanium implants: a review. Adv Eng Mater 2018;20:1700648. https://doi.org/10.1002/adem.201700648.

[12] Dewidar MM, Yoon HC, Lim JK. Mechanical properties of metals for biomedical applications using powder metallurgy process: a review. Met Mater Int 2006;12:193–206. https://doi.org/10.1007/BF03027531.

[13] Ryan G, Pandit A, Apatsidis DP. Fabrication methods of porous metals for use in orthopaedic applications. Biomaterials 2006;27:2651–70. https://doi.org/10.1016/j.biomaterials.2005.12.002.

[14] Zhang LC, Liu Y, Li S, Hao Y. Additive manufacturing of titanium alloys by electron beam melting: a review. Adv Eng Mater 2018;20:1700842. https://doi.org/10.1002/adem.201700842.

[15] Chen LY, Liang SX, Liu Y, Zhang LC. Additive manufacturing of metallic lattice structures: unconstrained design, accurate fabrication, fascinated performances, and challenges. Mater Sci Eng R Rep 2021;146:100648. https://doi.org/10.1016/j.mser.2021.100648.

[16] Committee AIH. Powder metal technologies and applications, 7. ASM International Handbook Committee; 1998.

[17] Wang JC, Liu YJ, Qin P, Liang SX, Sercombe TB, Zhang LC. Selective laser melting of Ti–35Nb composite from elemental powder mixture: microstructure, mechanical behavior and corrosion behavior. Mater Sci Eng, A 2019;760:214–24. https://doi.org/10.1016/j.msea.2019.06.001.

[18] Yılmaz E, Gökçe A, Findik F, Gulsoy HO, İyibilgin O. Mechanical properties and electrochemical behavior of porous Ti-Nb biomaterials. J Mech Behav Biomed Mater 2018;87:59–67. https://doi.org/10.1016/j.jmbbm.2018.07.018.

[19] Liu HW, Paul Bishop D, Plucknett KP. A comparison of Ti-Ni and Ti-Sn binary alloys processed using powder metallurgy. Mater Sci Eng, A 2015;644:392–404. https://doi.org/10.1016/j.msea.2015.07.085.

[20] Correa-rossi M, Romero-resendiz L, Leal-bayerlein D, Garcia-alves AL, Segovia-l F, Amigo V. Mechanical, corrosion, and ion release studies of Ti-34Nb-6Sn alloy with comparable to the bone elastic modulus by powder metallurgy method. Powders 2022;1:3–17. https://doi.org/10.3390/powders1010002.

[21] Lario J, Vicente Á, Amigó V. Evolution of the microstructure and mechanical properties of a Ti35Nb2Sn alloy post-processed by hot isostatic pressing for biomedical applications. Metals 2021;11:1027. https://doi.org/10.3390/met11071027.

[22] Yılmaz E, Gökçe A, Findik F, Özkan Gülsoy H. Characterization of biomedical Ti-16Nb-(0–4)Sn alloys produced by powder injection molding. Vacuum 2017;142:164–74. https://doi.org/10.1016/j.vacuum.2017.05.018.

[23] Romero-Resendiz L, Gómez-Sáez P, Vicente-Escuder A, Amigó-Borrás V. Development of Ti-In alloys by powder metallurgy for application as dental biomaterial. J Mater Res Technol 2021;11:1719–29. https://doi.org/10.1016/j.jmrt.2021.02.014.

[24] Xu W, Liu Z, Lu X, Tian J, Chen G, Liu B, et al. Porous Ti-10Mo alloy fabricated by powder metallurgy for promoting bone regeneration. Sci China Mater 2019;62:1053–64. https://doi.org/10.1007/s40843-018-9394-9.

[25] Mohan P, Rajak DK, Pruncu CI, Behera A, Amigó-Borrás V, Elshalakany AB. Influence of β-phase stability in elemental blended Ti-Mo and Ti-Mo-Zr alloys. Micron 2021;142:102992. https://doi.org/10.1016/j.micron.2020.102992.

[26] Yılmaz E, Gökçe A, Findik F, Gulsoy HÖ. Assessment of Ti–16Nb–xZr alloys produced via PIM for implant applications. J Therm Anal Calorim 2018;134:7–14. https://doi.org/10.1007/s10973-017-6808-0.

[27] Hafeez N, Liu J, Wang L, Wei D, Tang Y, Lu W, et al. Superelastic response of low-modulus porous beta-type Ti-35Nb-2Ta-3Zr alloy fabricated by laser powder bed fusion. Addit Manuf 2020;34:101264. https://doi.org/10.1016/j.addma.2020.101264.

[28] Liu YJ, Li SJ, Wang HL, Hou WT, Hao YL, Yang R, et al. Microstructure, defects and mechanical behavior of beta-type titanium porous structures manufactured by electron beam melting and selective laser melting. Acta Mater 2016;113:56–67. https://doi.org/10.1016/j.actamat.2016.04.029.

[29] Olivares-Navarrete R, Olaya JJ, Ramírez C, Rodil SE. Biocompatibility of niobium coatings. Coatings 2011;1:72–87. https://doi.org/10.3390/coatings1010072.

[30] Li Y, Wong C, Xiong J, Hodgson P, Wen C. Cytotoxicity of titanium and titanium alloying elements. J Dent Res 2010;89:493–7. https://doi.org/10.1177/0022034510363675.

[31] Hornez JC, Lefèvre A, Joly D, Hildebrand HF. Multiple parameter cytotoxicity index on dental alloys and pure metals. Biomol Eng 2002;19:103–17. https://doi.org/10.1016/S1389-0344(02)00017-5.

[32] Lee BH, Kim Y Do, Lee KH. XPS study of bioactive graded layer in Ti-In-Nb-Ta alloy prepared by alkali and heat treatments. Biomaterials 2003;24:2257–66. https://doi.org/10.1016/S0142-9612(03)00034-6.

[33] Calin M, Helth A, Gutierrez Moreno JJ, Bönisch M, Brackmann V, Giebeler L, et al. Elastic softening of β-type Ti-Nb alloys by indium (In) additions. J Mech Behav Biomed Mater 2014;39:162–74. https://doi.org/10.1016/j.jmbbm.2014.07.010.
[34] Pilz S, Gebert A, Voss A, Oswald S, Göttlicher M, Hempel U, et al. Metal release and cell biological compatibility of beta-type Ti-40Nb containing indium. J Biomed Mater Res Part B Appl Biomater 2018;106:1686–97. https://doi.org/10.1002/jbm.b.33976.
[35] Gebert A, Oswald S, Helth A, Voss A, Gostin PF, Rohnke M, et al. Effect of indium (In) on corrosion and passivity of a beta-type Ti-Nb alloy in Ringer's solution. Appl Surf Sci 2015;335:213–22. https://doi.org/10.1016/j.apsusc.2015.02.058.
[36] Li YH, Chen RB, xia Qi G, Wang ZT, Deng ZY. Powder sintering of porous Ti-15Mo alloy from TiH2 and Mo powders. J Alloys Compd 2009;485:215–8. https://doi.org/10.1016/j.jallcom.2009.06.003.
[37] Wang K. The use of titanium for medical applications in the USA. Mater Sci Eng, A 1996;213:134–7. https://doi.org/10.1016/0921-5093(96)10243-4.
[38] Radovic M, Lara-Curzio E, Riester L. Comparison of different experimental techniques for determination of elastic properties of solids. Mater Sci Eng, A 2004;368:56–70. https://doi.org/10.1016/j.msea.2003.09.080.
[39] Goldstein LS, Dewhirst MW, Repacholi M, Kheifets L. Summary, conclusions and recommendations: adverse temperature levels in the human body. Int J Hyperther 2003;19:373–84. https://doi.org/10.1080/0265673031000090701.
[40] The Materials Information Society. ASM handbook - alloy phase diagrams, 3; 1992.
[41] Gulay LD, Schuster JC. Investigation of the titanium–indium system. J Alloys Compd 2003;360:137–42. https://doi.org/10.1016/S0925-8388(03)00319-0.
[42] Aydogmus T, Al-Zangana NJF, Kelen F. Processing of β-type biomedical Ti74Nb26 alloy by combination of hot pressing and high temperature sintering. Konya J Eng Sci 2020;8:269–81. https://doi.org/10.36306/konjes.587790.
[43] Tang P, Puri VM. Methods for minimizing segregation: a review. Part Sci Technol 2004;22:321–37. https://doi.org/10.1080/02726350490501420.
[44] Hon YH, Wang JY, Pan YN. Composition/phase structure and properties of titanium-niobium alloys. Mater Trans 2003;44:2384–90. https://doi.org/10.2320/matertrans.44.2384.
[45] Robertson IM, Schaffer GB. Review of densification of titanium based powder systems in press and sinter processing. Powder Metall 2010;53:146–62. https://doi.org/10.1179/174329009X434293.
[46] Banerjee S, Mukhopadhyay P. Phase transformations: examples from titanium and zirconioum alloys. Elsevier; 2007.
[47] Han MK, Im JB, Hwang MJ, Kim BJ, Kim HY, Park YJ. Effect of indium content on the microstructure, mechanical properties and corrosion behavior of titanium alloys. Metals 2015;5:850–62. https://doi.org/10.3390/met5020850.
[48] Salib M, Teixeira J, Germain L, Lamielle E, Gey N, Aeby-Gautier E. Influence of transformation temperature on microtexture formation associated with α precipitation at β grain boundaries in a β metastable titanium alloy. Acta Mater 2013;61:3758–68. https://doi.org/10.1016/j.actamat.2013.03.007.
[49] Song B, Chen Y, Xiao W, Zhou L, Ma C. Formation of intermediate phases and their influences on the microstructure of high strength near-β titanium alloy. Mater Sci Eng, A 2020;793:139886. https://doi.org/10.1016/j.msea.2020.139886.
[50] Romero-Resendiz L, Cabrera JM, Elizalde S, Figueroa IA, Gonzalez G. Mechanical, stress corrosion cracking and crystallographic study on flat components processed by two combined severe plastic deformation techniques. J Mater Res Technol 2022;18:1281–94. https://doi.org/10.1016/j.jmrt.2022.03.010.
[51] Ji X, Gutierrez-Urrutia I, Emura S, Liu T, Hara T, Min X, et al. Twinning behavior of orthorhombic-α" martensite in a Ti-7.5Mo alloy. Sci Technol Adv Mater 2019;20:401–11. https://doi.org/10.1080/14686996.2019.1600201.
[52] Li C, Li G, Yang Y, Varlioglu M, Yang K. Martensitic twinning in Alpha + beta Ti-3.5Al-4.5Mo titanium alloy. J Metall 2011;2011:1–5. https://doi.org/10.1155/2011/924032.
[53] Rho JY, Kuhn-Spearing L, Zioupos P. Mechanical properties and the hierarchical structure of bone. Med Eng Phys 1998;20:92–102. https://doi.org/10.1016/S1350-4533(98)00007-1.
[54] Amigó-Mata A, Haro-Rodriguez M, Vicente-Escuder Á, Amigó-Borrás V. Development of Ti–Zr alloys by powder metallurgy for biomedical applications. Powder Metall 2022;65:31–8. https://doi.org/10.1080/00325899.2021.1943182.
[55] Bram Dr M, Ebel Dr T, Wolff M, Cysne Barbosa Dr AP, Tuncer Dr N. Applications of powder metallurgy in biomaterials. 2013. https://doi.org/10.1533/9780857098900.4.520.
[56] Zysset PK, Guo XE, Ho CE, Moore KE, Goldstein SA. Elastic modulus and hardness of cortical and trabecular bone lamellae measured by nanoindentation in the human. femur 1999;32:1005–12.
[57] Tendero I, Rossi MC, Viera M, Amado JM, Tobar MJ, Vicente Á, et al. Laser surface modification in Ti-xNb-yMo alloys prepared by powder metallurgy. Metals 2021;11:367. https://doi.org/10.3390/met11020367.
[58] Cremasco A, Ferreira I, Caram R. Effect of heat treatments on mechanical properties and fatigue resistance of Ti-35Nb alloy used as biomaterial. Mater Sci Forum 2010;636–637:68–75. https://doi.org/10.4028/www.scientific.net/MSF.636-637.68.
[59] Romero-Resendiz L, Rossi MC, Alvarez A, García-García A, Milian L, Tormo-Mas MA, et al. Microstructural, mechanical , electrochemical, and biological studies of an electron beam melted Ti-6Al-4V alloy. Mater Today Commun 2022;31:103337. https://doi.org/10.1016/j.mtcomm.2022.103337.
[60] Liao H, Wurtz T, Li J. Influence of titanium ion on mineral formation and properties of osteoid nodules in rat calvaria cultures. J Biomed Mater Res 1999;47:220–7. https://doi.org/10.1002/(SICI)1097-4636 (199911)47:2<220::AID-JBM12>3.0.CO;2-9.
[61] Schmalz G, Arenholt-Bindslev D, Pfüller S, Schweikl H. Cytotoxicity of metal cations used in dental cast alloys. ATLA, Altern Lab Anim 1997;25:323–30. https://doi.org/10.1177/026119299702500313.
[62] Wataha JC, Hanks CT, Craig RG. The in vitro effects of metal cations on eukaryotic cell metabolism. J Biomed Mater Res 1991;25:1133–49. https://doi.org/10.1002/jbm.820250907.
[63] Caicedo M, Jacobs JJ, Reddy A, Hallab NJ. Analysis of metal ion-induced DNA damage, apoptosis, and necrosis in human (Jurkat) T-cells demonstrates Ni2+ and V3+ are more toxic than other metals: Al3+, Be2+, Co2+, Cr 3+, Cu2+, Fe3+, Mo5+, Nb 5+, Zr2+. J Biomed Mater Res, Part A 2008;86:905–13. https://doi.org/10.1002/jbm.a.31789.
[64] Alfantazi AM, Moskalyk RR. Processing of indium: a review. Miner Eng 2003;16:687–94. https://doi.org/10.1016/S0892-6875(03)00168-7.
[65] Ralston KD, Birbilis N. Effect of grain size on corrosion: a review. Corrosion 2010;66:750051–7500513. https://doi.org/10.5006/1.3462912.

[66] Atapour M, Pilchak AL, Frankel GS, Williams JC. Corrosion behavior of β titanium alloys for biomedical applications. Mater Sci Eng C 2011;31:885–91. https://doi.org/10.1016/j.msec.2011.02.005.
[67] Fojt J, Joska L. Influence of porosity on corrosion behaviour of Ti-39Nb alloy for dental applications. Bio Med Mater Eng 2013;23:183–95. https://doi.org/10.3233/bme-130743.
[68] Rossi MC, de Santi Gouvêa E, Rodríguez MVH, Saeki MJ, Escuder AV, Borrás VA. Study of the current density of the electrical resistance sintering technique on microstructural and mechanical properties in a β Ti-Nb-Sn ternary alloy. Appl Phys Mater Sci Process 2021;127:1–19. https://doi.org/10.1007/s00339-021-04937-4.
[69] Yang J, Yang H, Yu H, Wang Z, Zeng X. Corrosion behavior of additive manufactured Ti-6Al-4V alloy in NaCl solution. Metall Mater Trans A Phys Metall Mater Sci 2017;48:3583–93. https://doi.org/10.1007/s11661-017-4087-9.
[70] Czarnowska E, Wierzchoń T, Maranda-Niedbała A. Properties of the surface layers on titanium alloy and their biocompatibility in in vitro tests. J Mater Process Technol 1999;92(93):190–4. https://doi.org/10.1016/S0924-0136(99)00228-9.